Comput Mech (2008) 41:219–229
DOI 10.1007/s00466-007-0180-z

ORIGINAL PAPER

Numerical investigation of dynamic shear bands in inelastic solids as a problem of mesomechanics

Adam Glema · Tomasz Łodygowski · Piotr Perzyna

Received: 7 December 2006 / Accepted: 4 April 2007 / Published online: 22 May 2007

Abstract The main objective of the present paper is to discuss very efficient procedure of the numerical investigation of the propagation of shear band in inelastic solids generated by impact-loaded adiabatic processes. This procedure of investigation is based on utilization the finite element method and ABAQUS system for regularized thermo-elasto-viscoplastic constitutive model of damaged material. A general constitutive model of thermo-elasto-viscoplastic polycrystalline solids with a finite set of internal state variables is used. The set of internal state variables is restricted to only one scalar, namely equivalent inelastic deformation. The equivalent inelastic deformation can describe the dissipation effects generated by viscoplastic flow phenomena. As a numerical example we consider dynamic shear band propagation in an asymmetrically impact-loaded prenotched thin plate. The impact loading is simulated by a velocity boundary condition, which are the results of dynamic contact problem. The separation of the projectile from the specimen, resulting from wave reflections within the projectile and the specimen, occurs in the phenomenon. A thin shear band region of finite width which undergoes significant deformation and temperature rise has been determined. Shear band advance, shear band velocity and the development of the temperature field as a function of time have been determined. Qualitative comparison of numerical results with experimental observation data has been presented. The numerical results obtained have proven the usefulness of the thermo-elasto-viscoplastic theory in the investigation of dynamic shear band propagations.

A. Glema · T. Łodygowski (✉)
Institute of Structural Engineering,
Poznań University of Technology, Piotrowo 5,
60-965 Poznań, Poland
e-mail: Tomasz.Lodygowski@put.poznan.pl

P. Perzyna
Institute of Fundamental Technological Research,
Polish Academy of Sciences, Świętokrzyska 21,
00-049 Warsaw, Poland

1 Prologue

In technological processes fracture can occur as a result of an adiabatic shear band localization generally attributed to a plastic instability generated by thermal softening and intrinsic microdamage mechanisms within a material.

Recent experimental observations have shown that the shear band procreates in a region of a body deformed where the resistance to plastic deformation is lower and the predisposition for localized shear band formation is higher. It has been found experimentally that in dynamic processes the shear band regions behave differently than adjacent zones. Within the shear band region the deformation process is characterized by very large strains (shear band strains over 100%) and very high strain rates (10^4–10^6 s^{-1}). The strain rate sensitivity of a material becomes very important feature of the shear band region.

The main objective of the present paper is to discuss very efficient procedure of the numerical investigation of the propagation of shear bands in inelastic solids generated by impact-loaded adiabatic processes, cf. [8,9].

This procedure of investigation is based on utilization the finite element method and ABAQUS system for regularized thermo-elasto-viscoplastic constitutive model of damaged material.

A general constitutive model of thermo-elasto-viscoplastic polycrystalline solids with a finite set of internal state variables is used. The set of internal state variables consists of one scalar, namely equivalent inelastic deformation. The equivalent inelastic deformation can describe the dissipation effects

generated by viscoplastic flow phenomena. The relaxation time is used as a regularization parameter.

The identification procedure for the material functions and constants involved in the constitutive equations is developed basing on the experimental observations of adiabatic shear bands in a HY-100 steel presented by Cho et al. [2].

As a numerical example let us consider dynamic shear band propagation in an asymmetrically impact-loaded pre-notched thin plate. The plate is made of a HY-100 steel. A notch (260 μm wide) is further extended by 2 mm and is situated symmetrically on the edge. The specimen is supported at four points and is initially stationary. The constant velocity $V_0 = 38$ m/s is imposed for projectile. The projectile comes into contact with the specimen over the width of 50 mm. The results of shear band advance and the changes of its velocity in time are presented in Figs. 1 and 2, respectively.

The impact loading is simulated by a velocity boundary condition which are the results of dynamic contact problem. The velocity imposed in specimen in front of projectile increases during the process. The separation of the projectile from the specimen, resulting from wave reflections within the projectile and the specimen, occurs in the phenomenon. All surface areas have traction free boundary conditions except where the velocity boundary condition is applied. We idealize the initial boundary value problem observed experimentally in Guduru et al. [10], by assuming the velocity boundary condition and different material of the specimen. The discretization parameters are assumed in such a way, to solve the problem of mesomechanics properly. The dimension of the accepted mesh is of the order 20 μm. A thin shear band region of finite width which undergoes significant deformation and temperature rise has been determined. Shear band advance, shear band velocity and the development of the temperature field as a function of time have been determined. Qualitative comparison of numerical results with experimental observation data has been presented. The numerical results obtained have proven the usefulness of the thermo-elasto-viscoplastic theory in the numerical investigation of dynamic shear band propagation.

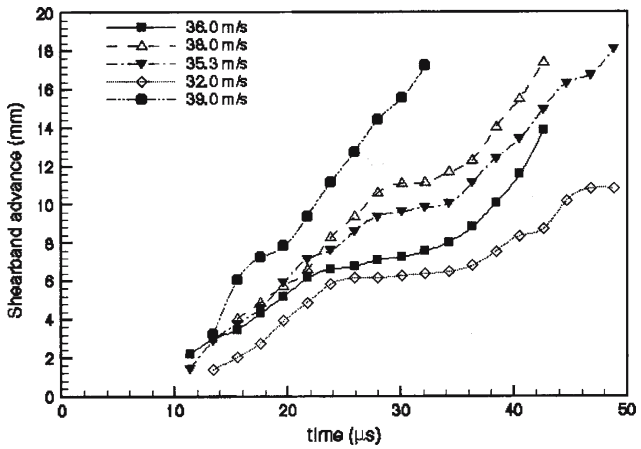

Fig. 1 Shear band advance as a function of time. (After [10])

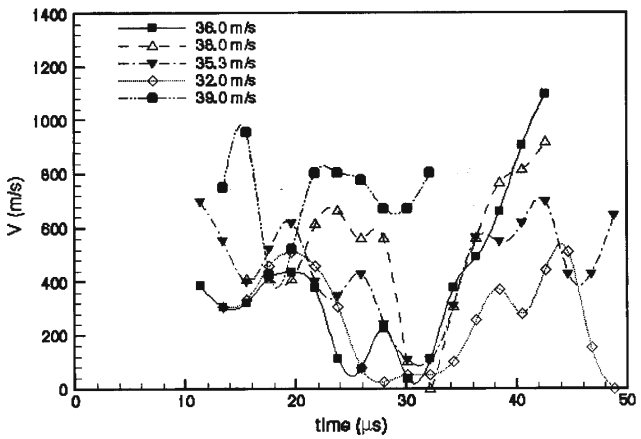

Fig. 2 Shear band velocity as a function of time. (After [10])

2 Physical and experimental motivation

2.1 Analysis of mesomechanical problems

In modern technology we observe recently very important application of metals, ceramics and polymers at mesoscale. Micromachines are in this size range clearly will be of increasing technological significance. Processes that control the mechanical integrity of microelectronic devices take also place on this size scale, cf. Needleman [14] and Hutchinson [11].

It is considerable experimental evidence that plastic flow and particularly localization of plastic deformation and fracture phenomena in crystalline solids are inherently size dependent over mesoscale range. It is generally accepted that: "smaller is stronger" or "smaller is harder".

Plastic behaviour at mesoscale range can not be characterized by conventional plasticity theories because they incorporate no material length scale and predict no size effect.

In recent years a variety of theoretical frameworks is emerging to describe inelastic deformation at the mesoscale. Four such frameworks (constitutive structures), each involving a length scale, are as follows: (1) discrete dislocation plasticity; (2) non-local plasticity; (3) the coupling of matter diffusion and deformation; (4) elasto-viscoplasticity.

The mesomechanical problems pose also numerical challenges. Computations on smaller size scale require smaller time steps. Since size dependent phenomena come into play when there are gradients of deformation and stress, hence numerical methods are usually needed to obtain solutions. Finite strains and rotations have to be taken into consideration.

At the mesoscale problems the dominant numerical methods are the finite element and finite difference methods.

It is noteworthy to add that the mesoscale continuum mechanics is in an early stage of development, both in terms of the theoretical framework as well as the computational methods.

In our consideration we shall use the thermo-elasto-viscoplasticity as a constitutive model of the material and apply the finite element method in numerical computations.

2.2 Experimental investigation of the initiation and propagation of shear bands

Guduru et al. [10] presented an experimental investigation of the initiation and propagation characteristics of dynamic shear band in C300 maraging steel. An elastic discharge machining (EDM) notch (260 μm wide) was further extended by 2 mm by fatigue loading.

In experimental investigation of Guduru et al. [10], two diagnostic techniques were used to observe the crack tip, the propagating shear band and the temperature field evolution during the initiation and propagation of the shear band. On one side of the specimen, the optical technique of coherent gradient sensing (CGS) in reflection was used to monitor the evolution of the stress intensity factors as a function of time. On the other side of specimen, a newly developed full-field, high-speed infrared (IR) imaging system was employed to measure the evolution, 2D-temperature field. They measure the advance of the shear band and its velocity in five different experiments, cf. Figs. 1 and 2. The shear band velocity can be seen to be highly transient and a function of the impact speed. In all but one experiment, the band arrests momentarily at about 30 μs, before accelerating to high speeds. The maximum shear band velocity observed here is about 1,100 m/s, cf. also Zhra et al. [23,24].

2.3 Fracture phenomena along localized shear bands

Fractured specimens were examined using an optical microscope to study the features of the shear bands such as its width, trajectory, the fracture surface, etc. The shear band is revealed as a white stripe. The thickness of the band is about 40 μm. A scanning electron microscope (SEM) image of the specimen surface that failed by shear band propagation, shows elongated voids, with sheared edges that are characteristic of such a failure mode. The presence of voids reveals the development of triaxiality tensile stress state that led to void growth and eventual fracture.

2.4 Temperature measurement

Guduru et al. [10] performed also broad experimental observations of the temperature field evolution during the initiation and propagation of the shear band. One of their objectives of imaging the temperature field was to visualize the development of the plastic zone at the tip of the initial crack and to observe its evolution, through further localization, into a shear band. The IR camera was focussed at the tip of the fatigue crack as illustrated on the left-hand side of Fig. 3. The impact speed was 35 m/s. They show a sequence of thermal images revelling the development of the temperature field as a function of time. Starting at about 21 μs, the central hot region extends to the right, as indicated by the contour lines, signifying the process of shear localization. The measured highest temperature rise within the plastic zone when this happened was at least 80 K, cf. Fig. 3.

Let us now focus our attention on the temperature field associated with the tip of a propagating shear band. The gradual nature of temperature rise at the front end of shear band supports the notion of a very diffuse shear band tip, as

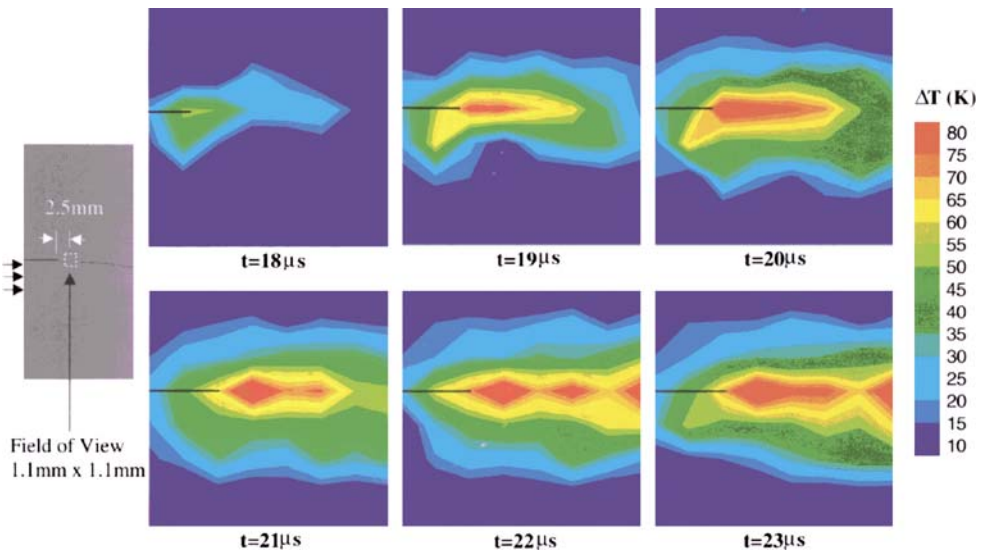

Fig. 3 A sequence of thermal images showing the transition of crack tip plastic zone into a shear band. (After [10])

opposed to a crack tip which carries a strong singularity in the field quantities.

As the shear band propagates, the material within the band progressively accumulates large plastic shear strains within short times and the temperature can quickly reach very high value. Of special interest in the investigation of Guduru et al. [10] has been the temperature distribution along a well-defined shear band. They have been consistently observed, in all experiments where a propagating shear band was imaged, that the temperature distribution along the band is highly non-uniform, with discrete regions of high temperature, that look like "hot spots". These hot spots are also seen to translate along the length of the band.

3 Formulation of the evolution problem

3.1 Thermodynamic theory of elasto-viscoplasticity

We shall use a constitutive model of elasto-viscoplastic polycrystalline solids developed within the thermodynamic framework of the rate type covariance structure with a finite set of the internal state variables (cf. [3–6,15–22]).

It is postulated that the internal state vector $\boldsymbol{\mu}$ has the form $\boldsymbol{\mu} = (\in^p)$, where $\in^p = \int_0^t \left(\frac{2}{3}\mathbf{d}^p : \mathbf{d}^p\right)^{\frac{1}{2}}$ defines the equivalent deformation and describes the dissipation effects generated by viscoplastic phenomena. The rate type constitutive equations for Kirchhoff stress tensor $\boldsymbol{\tau}$ and temperature ϑ have the form as follows

$$\begin{aligned} \mathrm{L}_{\boldsymbol{\upsilon}}\boldsymbol{\tau} &= \mathcal{L}^e : \mathbf{d} - \mathcal{L}^{\mathrm{th}}\dot{\vartheta} - \left[(\mathcal{L}^e + \mathbf{g}\boldsymbol{\tau} + \boldsymbol{\tau}\mathbf{g}) : \mathbf{P}\right] \\ &\quad \frac{1}{T_m}\left\langle \Phi\left(\frac{f}{\kappa} - 1\right)\right\rangle, \\ \rho c_p \dot{\vartheta} &= -\mathrm{div}\mathbf{q} + \vartheta\frac{\rho}{\rho_{Ref}}\frac{\partial \boldsymbol{\tau}}{\partial \vartheta} : \mathbf{d} + \rho\chi^*\boldsymbol{\tau} : \mathbf{d}^p, \end{aligned} \tag{1}$$

where $\mathrm{L}_{\boldsymbol{\upsilon}}$ denotes the Lie derivative and

$$\begin{aligned} &\mathcal{L}^e = \rho_{Ref}\frac{\partial^2\hat{\psi}}{\partial \mathbf{e}^2}, \qquad \mathcal{L}^{\mathrm{th}} = -\rho_{Ref}\frac{\partial^2\hat{\psi}}{\partial \mathbf{e}\partial\vartheta}, \\ &\psi = \hat{\psi}(\mathbf{e}, \mathbf{F}, \vartheta, \boldsymbol{\mu}), \qquad \mathbf{P} = \frac{\partial f}{\partial \boldsymbol{\tau}}\left(\left\|\frac{\partial f}{\partial \boldsymbol{\tau}}\right\|\right)^{-1}, \\ &f = f(J_2, \vartheta, \boldsymbol{\mu}), \qquad \kappa = \hat{\kappa}(\in^p, \vartheta). \end{aligned} \tag{2}$$

We interpret $\mathcal{L}^e$ as the elastic matrix, $\mathcal{L}^{\mathrm{th}}$ as the thermal expansion matrix, ψ is the free energy function, $\mathbf{F}$ denotes the deformation gradient, $\mathbf{e}$ is the total strain in the current configuration, ϑ denotes temperature, f is the plastic potential function, J_2 denotes the second invariant of the Kirchhoff stress tensor $\boldsymbol{\tau}$, T_m denotes the relaxation time for mechanical disturbances, κ is the isotropic work-hardening-softening function, $c_p = -\vartheta\frac{\partial^2\hat{\psi}}{\partial\vartheta^2}$ defines the specific heat, $\mathbf{q}$ denotes the heat flow vector field, $\mathbf{d} = \mathbf{d}^e + \mathbf{d}^p$ is the total deformation rate tensor, $\mathbf{g}$ denotes the metric tensor in the current configuration, Φ is the empirical overstress viscoplastic function, ρ_{Ref} and ρ denote the mass density in the reference and current configuration respectively, and χ^* is the irreversibility coefficient.

3.2 Initial-boundary value problem (evolution problem)

Find $\boldsymbol{\varphi}$ as function of t and $\mathbf{x}$ satisfying

$$\left.\begin{array}{ll} \text{(i)} & \dot{\boldsymbol{\varphi}} = \mathcal{A}(t, \boldsymbol{\varphi})\boldsymbol{\varphi} + \mathbf{f}(t, \boldsymbol{\varphi}); \\ \text{(ii)} & \boldsymbol{\varphi}(0) = \boldsymbol{\varphi}^0(\mathbf{x}); \\ \text{(iii)} & \text{The boundary conditions;} \end{array}\right\} \tag{3}$$

where the unknown $\boldsymbol{\varphi}$ takes values in a Banach space, $\mathcal{A}(t, \boldsymbol{\varphi})$ is a spatial linear differential operator (in general unbounded) depending on t and $\boldsymbol{\varphi}$, $\mathbf{f}$ is a nonlinear function, and the dot denotes the material derivative.

The evolution problem (3) describes an adiabatic inelastic flow process provided

$$\boldsymbol{\varphi} = \begin{bmatrix} \boldsymbol{\upsilon} \\ \rho \\ \boldsymbol{\tau} \\ \vartheta \end{bmatrix}, \tag{4}$$

$$\mathbf{f} = \begin{bmatrix} 0 \\ 0 \\ -\frac{\langle\Phi(\frac{f}{\kappa}-1)\rangle}{T_m}\left[\left(\mathcal{L}^e + \frac{\chi^*\boldsymbol{\tau}}{\rho_{Ref}}\mathcal{L}^{\mathrm{th}} + \mathbf{g}\boldsymbol{\tau} + \boldsymbol{\tau}\mathbf{g}\right) : \mathbf{P}\right] \\ \frac{1}{T_m}\langle\Phi(\frac{f}{\kappa} - 1)\rangle\frac{\chi^*}{\rho_{Ref}}\mathcal{L}^{\mathrm{th}}\boldsymbol{\tau} : \mathbf{P} \end{bmatrix},$$

$$\mathcal{A} = \begin{bmatrix} 0 & \frac{\boldsymbol{\tau}}{\rho_{Ref}\rho}\mathrm{grad} & \frac{1}{\rho_{Ref}}\mathrm{div}\,0 \\ 0 & -\rho\mathrm{div} & 0 \quad 0 \\ 0 & \mathbb{E} : \mathrm{sym}\frac{\partial}{\partial\mathbf{x}} + 2\mathrm{sym}(\boldsymbol{\tau} : \frac{\partial}{\partial\mathbf{x}}) & 0 \quad 0 \\ 0 & \frac{\vartheta}{c_p\rho_{Ref}}\frac{\partial\boldsymbol{\tau}}{\partial\vartheta} : \mathrm{sym}\frac{\partial}{\partial\mathbf{x}} & 0 \quad 0 \end{bmatrix}.$$

where

$$\mathbb{E} = \mathcal{L}^e - \frac{\vartheta}{c_p\rho_{Ref}}\mathcal{L}^{\mathrm{th}}\frac{\partial\boldsymbol{\tau}}{\partial\vartheta} \tag{5}$$

denotes the thermo–elastodynamic matrix for adiabatic process and $\boldsymbol{\upsilon}$ is the spatial velocity.

3.3 Numerical solution of the evolution problem

The discretization in space and time based on the finite element method is developed. Rate dependency (viscosity) allows the spatial differential operator in the governing equations to retain hyperbolic and the initial value problem (the Cauchy problem) is well-posed. Viscosity introduces implicitly a length-scale parameter into the dynamical initial-boundary value problem.

The viscoplastic regularization procedure assures the stable integration algorithm by using the finite element method. Particular attention is focused on the well-posedness of the evolution problem (the initial-boundary value problem) as well as on its numerical solutions. The Lax–Richtmyer equivalence theorem is formulated and conditions under which this theory is valid are examined.

We take advantage of the Lax–Richtmyer equivalence theorem which says that if the evolution problem (3) is well posed for $t \in [0, t_0]$ and if it is approximated by the finite element scheme, which is consistent then the scheme is convergent to the strict solution of the evolution problem (3) if and only if it is stable.

In explicit finite element scheme for a set of the partial differential equations (3)(i) of the hyperbolic type the condition of stability is the criterion of Courant–Friedrichs–Lewy,

$$\Delta t_{n,n+1} \leq \min \left(\frac{\Delta L^n_{p,q,r}}{\left| c^n_{p,q,r} \right|} \right), \qquad (6)$$
$$p = 1, 2, 3, \ldots, P \quad q = 1, 2, 3, \ldots, Q;$$
$$r = 1, 2, 3, \ldots, R,$$

where $\Delta t_{n,n+1}$ denotes time step, $c^n_{p,q,r}$ denotes the velocity of the propagation of the disturbances in the vicinity of the central node (p, q, r), $\Delta L^n_{p,q,r}$ is the minimum distance between the mesh nodes which are in the vicinity of the node.

The Courant–Friedrichs–Lewy condition requires that the numerical domain of dependence of a finite-element scheme include the domain of dependence of the associated partial differential equations.

4 Identification procedure

4.1 Assumption of the material functions for an adiabatic process

Let us assume the plastic potential function for a material in the form

$$f = J_2, \quad \text{where} \quad J_2 = \frac{1}{2} \tau'^{ab} \tau'^{cd} g_{ac} g_{bd}. \qquad (7)$$

The isotropic hardening-softening material function κ is postulated in the form as follows

$$\kappa = \kappa_0^2 \left\{ \frac{\kappa_1}{\kappa_0} + \left(1 - \frac{\kappa_1}{\kappa_0} \right) \exp\left[-h(\vartheta) \in^p \right] \right\}^2 (1 - b\vartheta), \quad (8)$$

where κ_0 and κ_1 denote the yield and saturation stress of the matrix material, respectively, $h = h(\vartheta)$ is the temperature dependent strain hardening function and b is a material coefficient.

The overstress function Φ is assumed in the form

$$\Phi \left(\frac{f}{\kappa} - 1 \right) = \left(\frac{f}{\kappa} - 1 \right)^m, \qquad \text{where} \quad m = 1, 3, 5, \ldots \qquad (9)$$

4.2 Determination of the material constants

To determine the material constants assumed we take advantage of the experimental observations of adiabatic shear bands in a HY-100 steel presented by Cho et al. [2]. In this experiment the specimens used were machined in the shape of thin-walled tubes with integral hexagonal flanges for gripping. Torsional loading at high strain rates was applied in a torsional Kolsky bar (split-Hopkinson bar). Kolsky bar provides a relatively simple and uniform state of shear stress during dynamic deformation, because the instrumentation affords an easy means of measuring average strain as a function of time, and because supplementary instrumentation can be added easily to measure local strain and the temperature distribution.

From the observations we have the results as follows

(i) The room temperature dynamic shear stress–strain curve, as obtained with the torsional Kolsky bar.
(ii) The corresponding nominal strain rate was assumed constant and was about 1,200 s^{-1}.
(iii) The maximum shear strain at fracture in dynamic deformation is about 1,000%.
(iv) Shear bands were examined using optical microscopy, Fig. 5, polarized light microscopy, and SEM. Shear band area is white after etching and its edges are relatively well-defined with different surface features apparent within the shear band area and the matrix material. The average width of the shear band is approximately 20 μm, the maximum local shear strain is about 1,000%, and the maximum temperature is about 590°C.
(v) The formation of a shear band during the test of a HY–100 steel specimen has been investigated by a high speed image converter camera and is clearly shown in Figs. 6 and 7.
(vi) The average velocity of the propagation shear band is estimated to be around 250/500 m s^{-1}.

Let us consider the adiabatic dynamic process for a thin-walled steel tube twisted at nominal rate 1,000 s^{-1}. In fact we idealize the initial-boundary value problem investigated by Chi et al. [1] and Cho et al. [2]. We take here advantage of our previous numerical investigation presented by Lodygowski and Perzyna [13].

We assume an elasto-visco-perfectly plastic material and a specimen in the shape of thin-walled tube, cf. Fig. 8. The

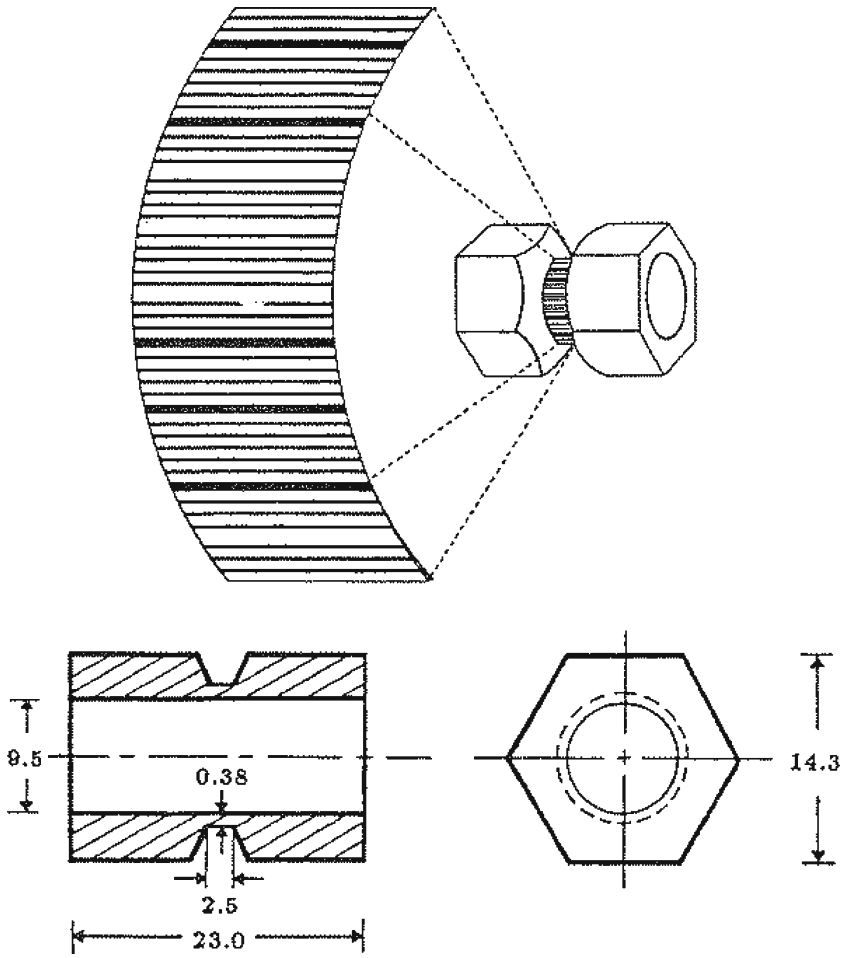

Fig. 4 Details of the thin-walled specimen with a blow–up of the fine grid deposited photographically on the outside surface of the specimen. The dimension are in milimeters (After [2])

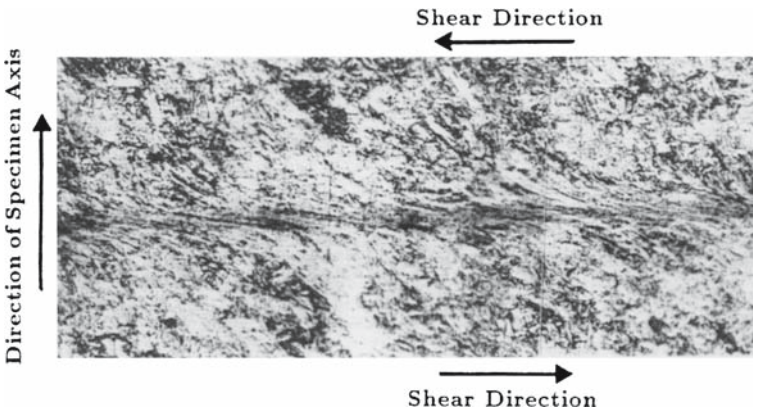

Fig. 5 Optical micrograph of a shear band formed in HY-100 steel, after polishing and etching (After [2])

bottom surface of the model is fixed to constrain the all possible displacements. The depth of thin wall tube (Figs. 8 and 9) is equal to 0.00125 m, which is half of measurement specimen length, cf. Fig 4 (for details see [7]). The top surface is the plane of symmetry of Split-Hopkinson Bar (SHB). At the surface the multipoint constraints (MPC) are introduced. To reflect the longitudinal stiffness and the mass of the specimen and SHB the single spring and concentrated mass is fixed to MPC. At the reference point of MPC the torsional loading is applied. It has been postulated that the specimen is twisted with $\omega^* = 253\ \mathrm{s}^{-1}$ and the duration of the process is 100 μs. The following values for various material parameters are assumed (HY-100 steel): density ρ = 7,830 kg/m^3, Young modulus $E = 208$ GPa, the specific heat $c_p = 460\ \mathrm{J\ kg^{-1}K^{-1}}$, the irreversible coefficient $\chi^* = 0.9$, the relaxation time $T_m = 2 \times 10^{-1}$ μs, $m = 1$, the yield stress $\kappa_0 = 598$ MPa for temperature 20°C, $\kappa_0 = 540$ MPa for temperature 100°C, $\kappa_0 = 483$ MPa for

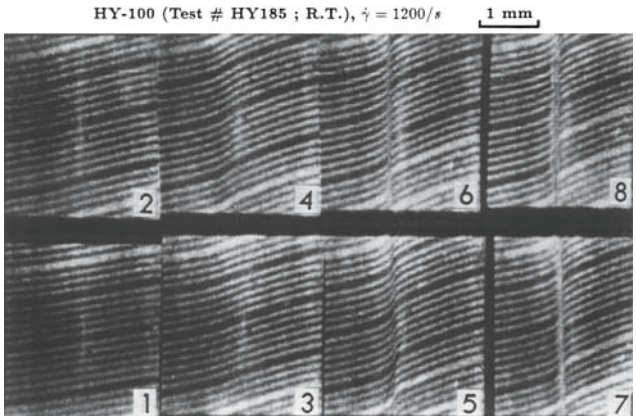

Fig. 6 Photographs of the grid pattern during the formation of a shear band in HY-100 steel taken by a high speed image converter camera. The time interval between frames is 40 μs (After [2])

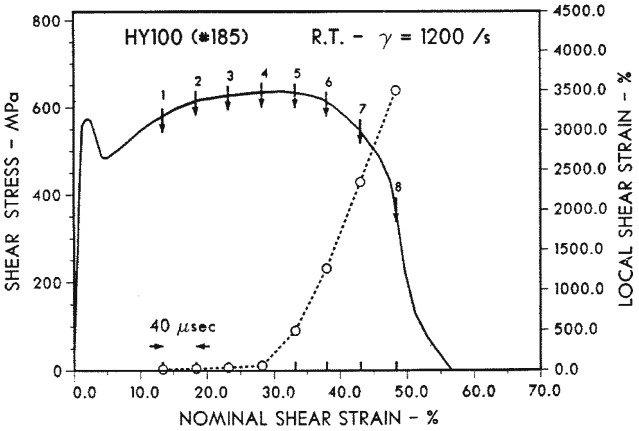

Fig. 7 The stress-strain behaviour of HY-100 steel. The number arrows indicate nominal strain values at which the photographs shown in Fig. 11 are taken. The corresponding values of the maximum local strain are shown by the dotted line (After [2])

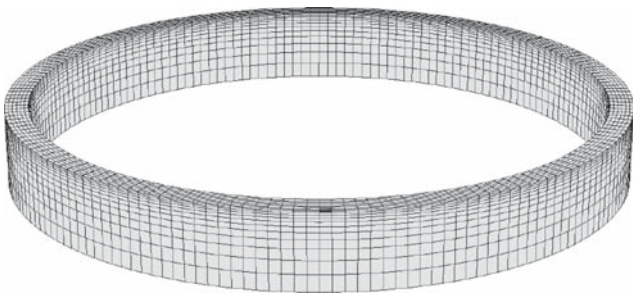

Fig. 8 Assumed model of the tube specimen for twisting

temperature 200°C, $\kappa_0 = 426$ MPa for temperature 300°C. An imperfection in the form of weaker material (Young modulus $E = 115$ GPa) has been introduced at one place near model top surface to initiate the shear band.

The shear band resulting from numerical simulation can propagate on the cylinder surface in different form, see Glema et al. [8,9]. It depends on longitudinal boundary and initial conditions used in the models. Here, it has been considered the solution in the ring form, cf. Fig. 9, when the shear band propagates in the plane orthogonal to longitudinal SHB axis. Detailed description of shear band propagation around the tube is presented in Glema et al. [8,9].

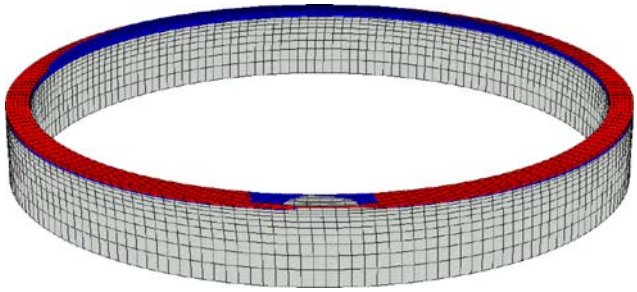

Fig. 9 Shear band propagation in the model of thin wall specimen under twisting

The shear band advance and the propagation velocity of the shear band as a function of time are shown in Fig. 10 (at the tip of shear band it has been assumed $\in^p = 0.25$). The average width of the shear band is obtained as 80/100 μm.

5 Numerical examples

5.1 Propagation of shear bands

In initial boundary value problem we idealize the process observed experimentally in Guduru et al. [10] and Li et al. [12] by assuming the velocity boundary condition and we define different material of the specimen (HY-100 steel).

A plane specimen of length 254 mm and width 95 mm has the initial notch at the center of the left edge. The thickness of the specimen is 12 mm. The notch length is 27.4 mm and the initial crack 2 mm long is present in the horizontal direction (see Fig. 11). The dimensions of the plate, notch and the initial crack are taken from experimental data. The supports and impact projectile position are also presented in Fig. 11. The projectile impacts the specimen with velocity equal to 38 m s^{-1}. There are two different positions of projectile giving the unsymmetric impact and symmetric one, when central impact is considered (dashed line in Fig. 11). For both positions of projectile the boundary conditions satisfy the symmetry by taking the same distance for upper and lower edge, but not the same at left (prenotched) and right side of the specimen.

The FE discretization is defined in such the way that finite element dimensions are of 20 μm in the region of interest. The whole model consists of 49,500 plain stress finite elements, 49,750 nodes, 99,500 degree of freedom.

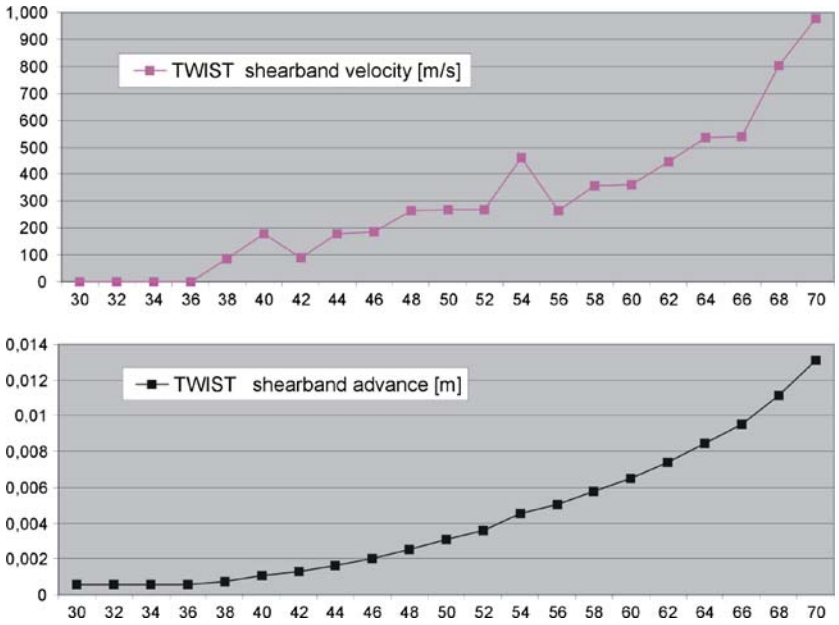

Fig. 10 Shear band velocity and shear band length as functions of time for twisting of tube

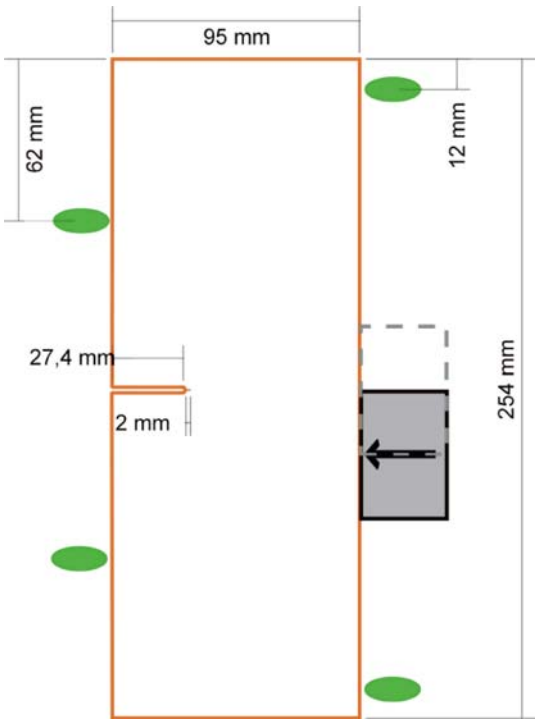

Fig. 11 Specimen geometry for impact of the plate

The contour plots of equivalent plastic strain and temperature obtained for time instants 40, 50, 60 μm are visualized in Fig. 12 for unsymmetric impact. Similar results for central impact are shown in Fig. 13.

To show better that we obtained non-uniform temperature distribution along the shear band for both considered cases we present the magnification of the results for the field of temperature at 60 μs for unsymmetric and central impacts, respectively, cf. Figs. 14 and 15. The contour value of 25% for plastic equivalent strain is taken to observe the shear band initiation and propagation. Putting down the coordinates of position of shear band advance and controlling the deformation during the process the functions of shear band length and propagation velocity of its front are calculated. That results are displayed in Fig. 16.

5.2 Discussion of the numerical results

The results of numerical simulation of shear band allow to observe the dynamic process of advance of shear band tip in material specimen under impact loading. The calculated values of equivalent inelastic deformation make possible to estimate shear band length advance and the velocity of shear band propagation. The period of time 40 μs is common for computed examples to report the shear band propagation, from its initiation to considered advance. Within the same time period formation of shear band is also observed in experimental measurement. The advances of shear band length in experiments and in computations have similar final values and functions presenting its evolution are comparable. The comparison of the shear band propagation velocity reaches the same conclusion. The calculated values of $200 - 500$ m s^{-1} for tube twisting and from 100 m s^{-1} up to value of 900 m s^{-1} for pre-notched plate example are of the range the experimental results. Rather the qualitative agreement of experimental simulation results is verified, than strict comparison of values.

The functions of the simulated shear band propagation velocity for pre-notched plate, like the functions obtained from laboratory test, show quite variant, but increase of its value at the beginning of shear band advance, later the sudden

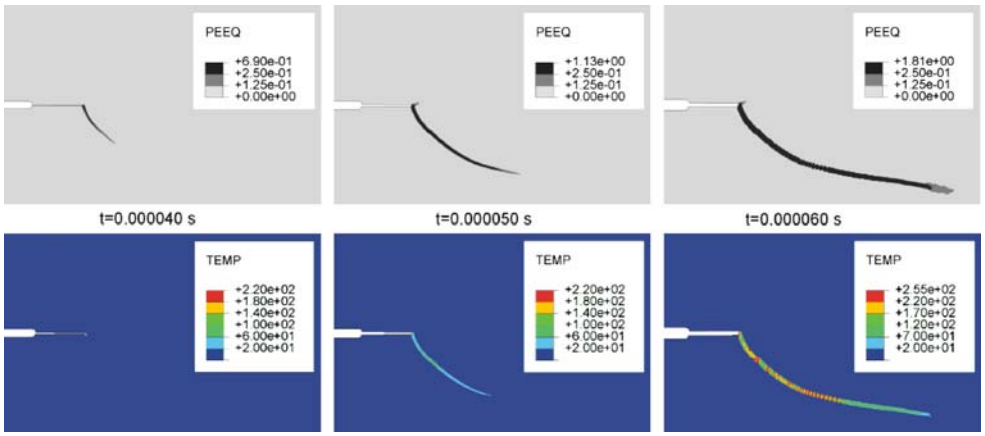

Fig. 12 Evolution of plastic equivalent deformation and temperature along the shear band for unsymmetric impact (for 40, 50, 60 μs)

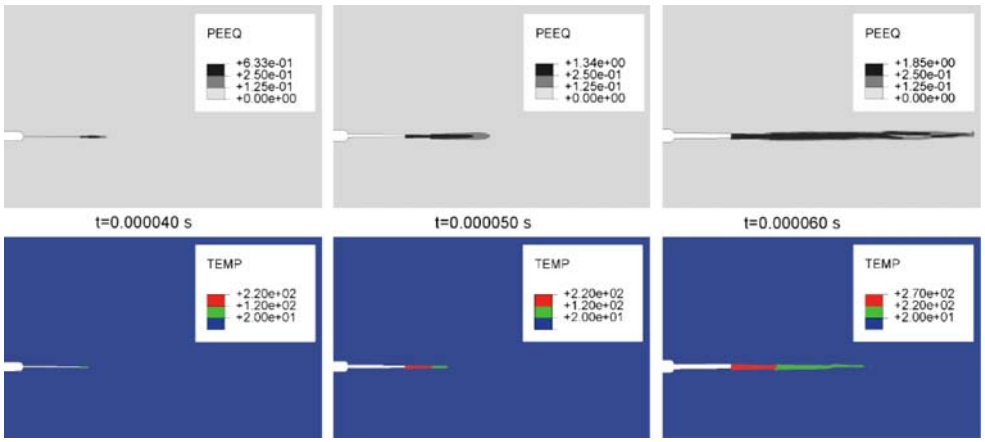

Fig. 13 Evolution of plastic equivalent deformation and temperature along the shear band for central impact (for 40, 50, 60 μs)

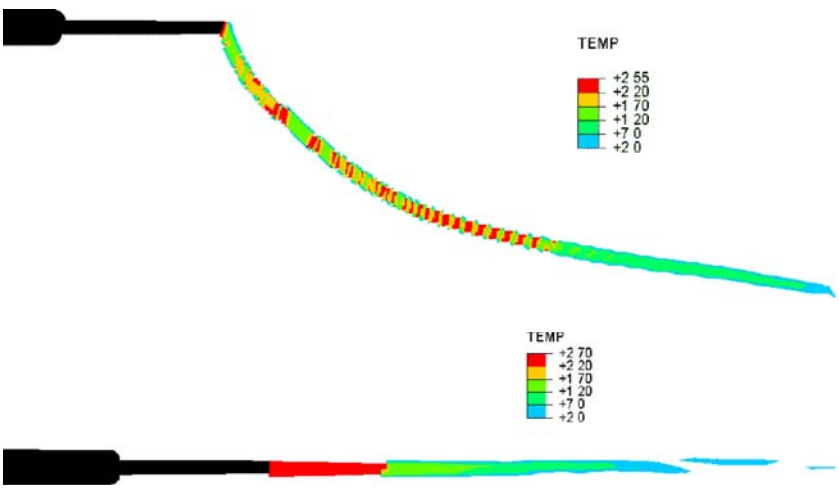

Fig. 14 Magnification of the results for the field of temperature at 60 μs for unsymmetric impact

Fig. 15 Magnification of the results for the field of temperature at 60 μs for central impact

drop of its value after reaching the maximum and one more increasing path at the end of time period. The common sudden velocity drop, observed in experiments and simulations, is specially worth to point it out. The calculation of velocity values using results from simulation is generally sensitive to the exactness of shear band tip evidence. Relatively small length of the shear band, together with the fact that material and boundary conditions do not correspond directly accent the qualitative agrement of results. The remark concerning the temperature results goes in the same direction. There is valuable to expose that numerical results show the particular character of experimental ones, with occurrence of discrete regions of high temperature, that are described as "hot spots". At the beginning of shear band advance the

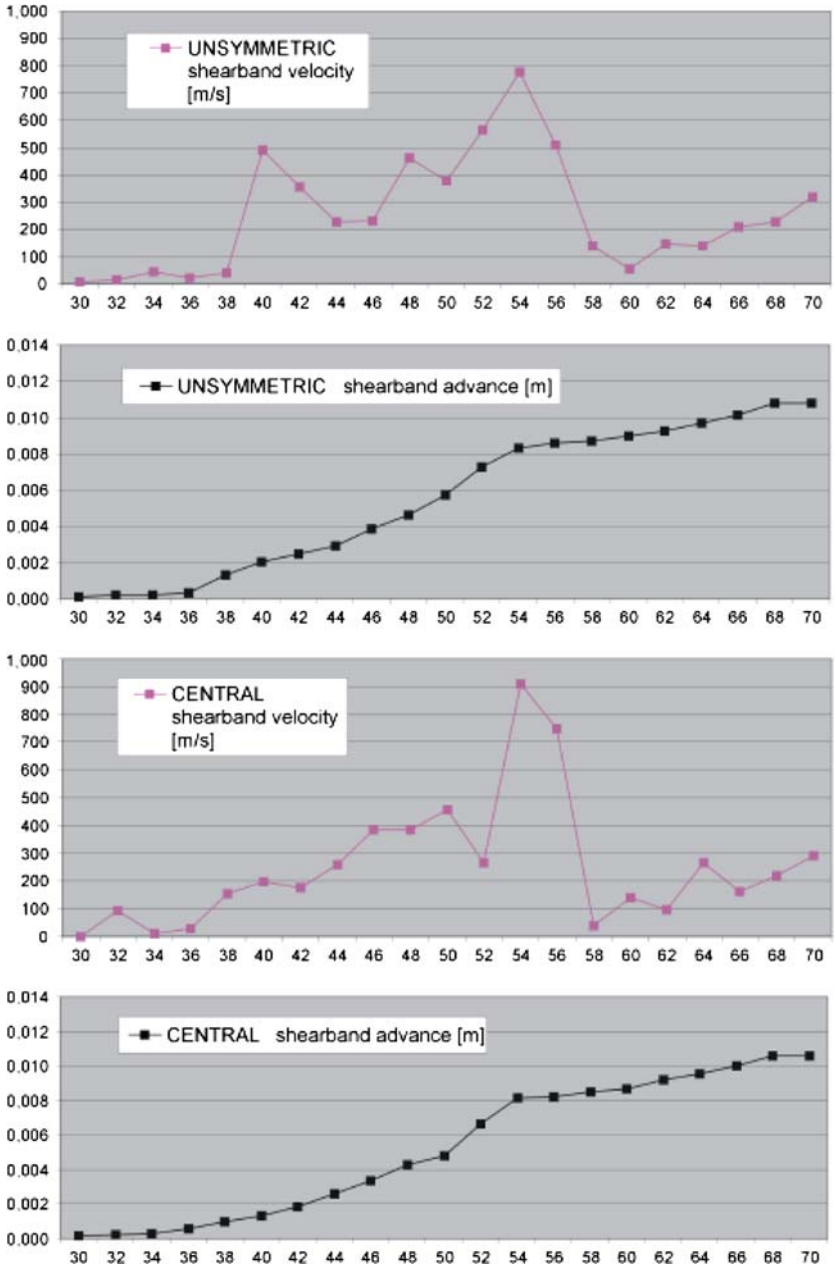

Fig. 16 Propagation velocity of shear band front and shear band length as functions of time, for unsymmetric and central impacts

temperature uniformly decreases around the crack tip, but next the temperature field changes the distribution and there is no more rule that temperature continuously is lower when the distance from maximum is greater. Appearance of several local extremes take place after the mentioned above drop of propagation velocity. The evolution of described variables suggests the step-wise nature of shear band propagation phenomena.

6 Epilogue

The elaborated numerical algorithm satisfies the material objectivity principle with respect to diffeomorphism (any motion). The discretization parameters are assumed in such a way that the problem of mesomechanics is solved properly. A thin shear band region of finite width which undergoes significant deformation and temperature rise has been determined. Its evolution until occurrence of final fracture has been simulated. Shear band advance, shear band velocity and the development of the temperature field as a function of time have been determined. Qualitative comparison of numerical results with experimental observation data has been presented. The numerical results obtained have been proven the usefulness of the thermo-elasto-viscoplastic theory in the numerical investigation of dynamic shear band propagation.

References

1. Chi YC, Lee SH, Cho K, Duffy J (1988) The effects of tempering and test temperatures on the dynamic fracture initiation behaviour of on AISI 4340 VAR steel. Brown University Technical Report, August
2. Cho K, Chi YC, Duffy J (1988) Microscopic observations of adiabatic shear bands in three different steels. Brown University Report No DAAL03-88-K-0015/3, September
3. Dornowski W, Perzyna P (2002) Numerical analysis of macrocrack propagation along a bimaterial interface under dynamic loading processes. Int J Solids Struct 39:4949–4977
4. Dornowski W, Perzyna P (2005) Numerical investigation of localized fracture phenomena in inelastic solids
5. Duszek MK, Perzyna P (1991) The localization of plastic deformation in thermoplastic solids. Int J Solids Struct 27:1419–1443
6. Duszek-Perzyna MK, Perzyna P (1994) Analysis of the influence of different effects on criteria for adiabatic shear band localization in inelastic solids. In: Batra RC, Zbib HM (eds) Proceedings material instabilities: theory and applications, ASME Congress, Chicago, 9–11 November 1994, AMD-vol 183/MD-vol 50, ASME, New York, pp 59–85
7. Glema A, Kakol W, Łodygowski T (1997) Numerical modelling of adiabatic shear band formation in a twisting test. Eng Trans 45(3–4):419–431
8. Glema A, Łodygowski T, Perzyna P (2004) Numerical investigation of dynamic shear bands in inelastic solids as a problem of mesomechanisc. International congress of theoretical and applied mechanics, 15–21 August 2004, Warsaw, Poland, 240 (+ CDROM)
9. Glema A, Łodygowski T, Perzyna P (2004) Estimation of shear band propagation velocity in metal specimens and failure phenomenon under impact loading VI world congress on computational mechanics in conjunction with APCOM'04, 5–10 September 2004, Beijing, China, Computational Mechanics (Abstracts), Tsinghua University Press & Springer, Heidelberg, 272 (+ CDROM)
10. Guduru PR, Rosakis AJ, Ravichandran G (2001) Dynamic shear bands: an investigation using high speed optical and infrared diagnostic. Mech Mater 33:371–402
11. Hutchinson JW (2000) Plasticity at the micron scale. Int J Solids Struct 37:225–238
12. Li S, Liu W-K, Qian D, Guduru PR, Rosakis AJ (2001) Dynamic shear band propagation and micro-structure of adiabatic shear band. Comput Methods Appl Mech Engng 191:73–92
13. Łodygowski T, Perzyna P (1997) Numerical modelling of localized fracture of inelastic solids in dynamic loading processes. Int J Numer Methods Eng 40:4137–4158
14. Needleman A (2000) Computational mechanics at the mesoscale. Acta Mater 48:105–124
15. Perzyna P (1963) The constitutive equations for rate sensitive plastic materials. Q Appl Math 20:321–332
16. Perzyna P (1966) Fundamental problems in viscoplasticity. Adv Appl Mech 9:343–377
17. Perzyna P (1971) Thermodynamic theory of viscoplasticity. Adv Appl Mech 11:313–354
18. Perzyna P (1986) Internal state variable description of dynamic fracture of ductile solids. Int J Solids Struct 22:797–818
19. Perzyna P (1986) Constitutive modelling for brittle dynamic fracture in dissipative solids. Arch Mech 38:725–738
20. Perzyna P (1995) Interactions of elastic-viscoplastic waves and localization phenomena in solids. In: Wegner JL, Norwood FR (eds) Proceedings IUTAM Symposium on Nonlinear Waves in Solids, August 15–20, 1993, Victoria, Canada, ASME 1995, pp 114–121
21. Perzyna P (1984) Constitutive modelling of dissipative solids for postcritical behaviour and fracture. ASME J Eng Mater Technol 106:410–419
22. Perzyna P (2001) Thermo-elasto-viscoplasticity and damage. In: Lemaitre J (ed) Handbook of Materials Behaviour Models. Academic, New York, pp 821–834
23. Zhou M, Rosakis AJ, Ravichandran G (1996) Dynamic propagating shear band in impact–loaded prenotched plates. I. Experimental investigations of temperature signatures and propagation speed. J Mech Phys Solids 44:981–1006
24. Zhou M, Ravichandran G, Rosakis AJ (1996) Dynamic propagating shear band in impact–loaded prenotched plates. II. Numerical simulations. J Mech Phys Solids 44:1007–1032